CP violation at ATLAS in effective field theory

Supratim Das Bakshi,[1,*] Joydeep Chakrabortty,[1,†] Christoph Englert,[2,‡] Michael Spannowsky,[3,§] and Panagiotis Stylianou[2,‖]

[1]*Indian Institute of Technology Kanpur, Kalyanpur, Kanpur 208016, India*
[2]*School of Physics & Astronomy, University of Glasgow, Glasgow G12 8QQ, United Kingdom*
[3]*Institute for Particle Physics Phenomenology, Durham University, Durham DH1 3LE, United Kingdom*

(Received 6 October 2020; accepted 3 February 2021; published 15 March 2021)

CP violation beyond the Standard Model (SM) is a crucial missing piece for explaining the observed matter-antimatter asymmetry in the Universe. Recently, the ATLAS experiment at the Large Hadron Collider performed an analysis of electroweak Zjj production, thereby excluding the SM locally at 95% confidence level in the measurement of *CP*-sensitive observables. We take the excess interpretation in terms of anomalous gauge-Higgs interactions at face value and discuss further steps that are required to scrutinize its origin. In particular, we discuss the relevance of multiboson production using adapted angular observables to show how they can be used to directly tension the reported Zjj excess in a more comprehensive analysis. To connect the excess to a concrete UV scenario for which the underlying assumptions of the Zjj analysis are valid, we identify vectorlike leptons as a candidate theory consistent with the observed *CP*-odd Wilson coefficient hierarchy observed by ATLAS. We perform a complete one-loop matching calculation to motivate further model-specific and correlated new physics searches. In parallel, we provide estimates of the sensitivity reach of the LHC's high luminosity phase for this particular scenario of *CP* violation in light of electroweak precision and Run-2 Higgs data. These provide strong constraints on the model's *CP*-even low-energy phenomenology, but also inform the size of the *CP*-odd SM deformation indirectly via our model hypothesis.

DOI: 10.1103/PhysRevD.103.055008

I. INTRODUCTION

The search for non-Standard Model (SM) sources of *CP* violation is a crucial missing piece in connecting the phenomenological success of the SM so far with its apparent shortcomings related to the observed baryon antibaryon asymmetry [1]. Searches for *CP* violation in various channels at the Large Hadron Collider (LHC) are therefore a key part of the ongoing experimental program (see, e.g., [2,3] for recent analyses in the context of Higgs physics).

In particular, ATLAS has recently performed a detailed analysis of electroweak $Z+2j$ production in Ref. [4], where it also interprets measurements in terms of effective field theory (EFT) deformations of the SM using dimension six *CP*-violating operators in the Warsaw basis [5],

$$Q_{\tilde{W}} = \epsilon^{abc}\tilde{W}^a_{\mu\nu}W^{b\nu\rho}W^{c\rho\mu}, \tag{1}$$

$$Q_{H\tilde{W}B} = (H^\dagger\tau^a H)\tilde{W}^a_{\mu\nu}B^{\mu\nu}, \tag{2}$$

where W, B denote the field strengths of weak $SU(2)_L$ and hypercharge $U(1)_Y$, H is the Higgs doublet, τ^a are the Pauli matrices, and the tilde refers to the dual field strength tensor $\tilde{X}_{\mu\nu} = \epsilon_{\mu\nu\delta\rho}X^{\delta\rho}/2$ ($X = W, B, G$). Using the effective Lagrangian

$$\mathcal{L} = \mathcal{L}_{\rm SM} + \frac{C_{\tilde{W}}}{\Lambda^2}Q_{\tilde{W}} + \frac{C_{H\tilde{W}B}}{\Lambda^2}Q_{H\tilde{W}B}, \tag{3}$$

ATLAS provides the observed 95% confidence level constraints on the following *CP*-violating operators [4]:

$$C_{\tilde{W}}\frac{\text{TeV}^2}{\Lambda^2} \in [-0.11, 0.14], \qquad C_{H\tilde{W}B}\frac{\text{TeV}^2}{\Lambda^2} \in [0.23, 2.34], \tag{4}$$

based on dimension six interference-only contributions arising from matrix elements

$$|\mathcal{M}|^2 = |\mathcal{M}_{\rm SM}|^2 + 2\,\text{Re}[\mathcal{M}_{\rm SM}\mathcal{M}^*_{\rm d6}(C_{\tilde{W}}, C_{H\tilde{W}B})]. \tag{5}$$

*sdbakshi@iitk.ac.in
†joydeep@iitk.ac.in
‡christoph.englert@glasgow.ac.uk
§michael.spannowsky@durham.ac.uk
‖p.stylianou.1@research.gla.ac.uk

This leads to asymmetries in P-sensitive distributions, such as the "signed" (according to rapidity) azimuthal angle difference of the tagged jets $\Delta\Phi_{jj}$. The benefit of such observables and the study of their asymmetries is that the CP-even deformations do not contribute to the exclusion constraints directly, which also extends to CP-even modifications arising from "squared" dimension six contributions. In Eq. (5), $\mathcal{M}_{d6}$ denotes the amplitude contribution from the operators of Eq. (1); thus, it is a linear function of $C_{\tilde{W}}/\Lambda^2, C_{H\tilde{W}B}/\Lambda^2$ (as we are keeping terms up to order $1/\Lambda^2$).

The constraint on the Wilson coefficient (WC) $C_{H\tilde{W}B}$ in Eq. (4) indicates a tension with the SM while the observed cross section agrees well with the SM expectation with 39.5 fb data [6–8]. This prompts us to the following interesting questions.

First, the tension of Eq. (4) seems to rule out the SM at an SM-compatible cross section. Experimental analyses of asymmetries are challenging, and systematics are crucial limiting factors of distribution shape analyses. Nonetheless, the result of Ref. [4] could indeed be the first glimpse of a phenomenologically required and motivated extension of the SM, thus deserving further experimental and theoretical scrutiny.

Second, limiting ourselves to a subset of the dimension six operators that could in principle contribute to physical process can be theoretically problematic, in particular when we wish to interpret the experimental findings in a truly model-independent fashion. While concrete UV scenarios can be expected to exhibit hierarchical Wilson coefficient patterns, it is not *a priori* clear that limiting oneself to anomalous gauge boson interactions has a broad applicability to UV scenarios.

Addressing these two questions from a theoretical and phenomenological perspective is the purpose of this work. In Sec. II, we motivate additional diboson analyses of the current $\mathcal{O}(100)$ fb^{-1} data set that will allow us to tension or support the results of Eq. (4) straightforwardly. This is particularly relevant as the ATLAS constraints amount to a large, and as it turns out nonperturbative, amount of CP violation associated with a single direction in the EFT parameter space. In Sec. III, we show that the ATLAS assumptions of considering two operators are consistent for models of vectorlike leptons, which cannot only reproduce a hierarchy $|C_{H\tilde{W}B}|/\Lambda^2 > |C_{\tilde{W}}|/\Lambda^2$ as suggested by Ref. [4], but also collapse the analysis-relevant operators to those modifying the gauge boson self-interactions for the considered analyses. Combining both aspects, in Sec. IV, we assess the future of diboson and $Z+2j$ analyses from a perturbative perspective and discuss the high-luminosity (HL) sensitivity potential of the LHC in light of the electroweak precision constraints. We conclude in Sec. V.

II. SCRUTINIZING $C_{H\tilde{W}B}$ WITH DIBOSON PRODUCTION AND CURRENT LHC DATA

Deviations related to the gauge boson self-coupling structure can be scrutinized using abundant diboson production at the LHC. With clear leptonic final states and large production cross sections, these signatures are prime candidates for electroweak precision analyses in the LHC environment with only a minimum of background pollution; see also [9,10]. In particular, radiation zeros observed in $W\gamma$ production are extremely sensitive to perturbations of the SM CP-even coupling structures [11–17]. In this section, we discuss the relevant processes that can be employed to further tension the findings of Eq. (4).

A. Processes

The squared amplitude of Eq. (5) receives interference contributions from dimension six operators that in the special case where they are CP odd, do not change the cross section of a process but appear in CP-sensitive observables. Anomalous weak boson interactions were studied in Ref. [4] through the Zjj channel by the introduction of two CP-violating operators, $Q_{\tilde{W}}$ and $Q_{H\tilde{W}B}$, modifying the differential distribution of the parity-sensitive signed azimuthal angle between the two final state jets $\Delta\phi_{jj} = \phi_{j_1} - \phi_{j_2}$, where ϕ_{j_1} (ϕ_{j_2}) is the azimuthal angle of the first (second) jet, as ordered by rapidity. Similar parity-sensitive observables can be constructed for the leptonic final states of the $W\gamma \to \ell\nu\gamma$, $W^+W^- \to \ell^+\nu_\ell\ell^-\bar{\nu}_\ell$, and $WZ \to \ell\nu\ell^+\ell^-$ channels allowing to further constrain the reach of the two Wilson coefficients.

The operators are modeled using FeynRules [18,19] and exporting the interactions through a UFO [20] file. Events are generated using MadEvent [21–23] through the MadGraph framework [23] and saved in the LHEF format [24] before imposing selection criteria and cuts.

1. WZ production at the LHC

We study the WZ channel by selecting leptons in the pseudorapidity $|\eta(\ell)| < 2.5$ and transverse momentum $p_T > 5$ GeV regions. Exactly three leptons are required and at least one same-flavor opposite-charge lepton pair must have an invariant mass within the Z boson mass window $m_{\ell\ell} \in [60, 120]$ GeV. In the case of more than one candidate pairs, the one that yields an invariant mass closest to the Z boson is selected. The remaining lepton ℓ' is required to have $p_T(\ell') > 20$ GeV. To obtain a P-sensitive observable, we reconstruct the dilepton pair four-momentum and obtain the rapidity $y_{\ell\ell}$ and azimuthal angle $\phi_{\ell\ell}$. We order the dilepton and third lepton azimuthal angles based on the rapidities of the two reconstructed objects, such that ϕ_1 (ϕ_2) is the one with the greatest

(smallest) rapidity. The signed azimuthal angle is then constructed as $\Delta\phi_{\ell' Z} = \phi_1 - \phi_2$.

The distributions of the signed azimuthal angle for both the SM and the SM-BSM (beyond the Standard Model) interference are normalized to the CMS measured fiducial cross section [25] of the particular phase space region at 13 TeV center of mass energy,

$$\sigma_{\text{fid}}(pp \to WZ \to \ell'\nu\ell\ell) = 258 \pm 21(\text{stat})^{+19}_{-20}(\text{syst}) \pm 8.0(\text{lumi})\ \text{fb}. \quad (6)$$

2. WW production at the LHC

Turning to the WW channel and following Ref. [26], we produce events decaying to the $WW \to e\nu_e\mu\nu_\mu$ final state. The two leptons e and μ are required to satisfy $|\eta(\ell)| < 2.5$ and $p_T(\ell) > 27$ GeV with no third lepton in the $p_T > 10$ GeV region. Contributions from the Drell-Yan background are reduced by imposing cuts on the missing energy $E_T > 20$ GeV and on the transverse momentum of the dilepton pair $p_T(e\mu) > 30$ GeV. The phase space region is constrained further by enforcing the invariant mass condition $m(e\mu) > 55$ GeV that suppresses the $H \to WW$ background. In this channel, the signed azimuthal angle $\Delta\phi_{\ell\ell}$ is then defined directly from the azimuthal angles of the two leptons sorted by rapidity.

The fiducial cross section of $WW \to e\mu + \not{E}_T$ was measured by ATLAS [26] as

$$\sigma_{\text{fid}}(pp \to WW \to \ell\nu_e\mu\nu_\mu) = 379.1 \pm 5.0(\text{stat}) \pm 25.4(\text{syst}) \pm 8.0(\text{lumi})\ \text{fb}, \quad (7)$$

which is used to normalize the calculated differential distribution of $\Delta\phi_{\ell\ell}$. The total cross section of the events and the relative statistical and systematic uncertainties are subsequently rescaled to include the final states of all light leptons $WW \to \ell\nu\ell\nu$.

3. Wγ production at the LHC

To obtain the cross section of $W\gamma$ at 13 TeV, we first use MCFM [27–31] with generation level cuts $p_T > 10$ GeV and $|\eta| < 2.5$ for both leptons and photons, requiring the separation $\Delta R(\ell,\gamma) > 0.4$, in order to obtain the cross section at next-to-leading order precision with $p_T(\gamma)$ as the renormalization and factorization scale. We have validated these choices against early measurements from ATLAS [9] and CMS [10]. The events are generated as before with MadEvent using the same generation cuts and we rescale the computed MadEvent cross section of the events to the MCFM value, in order to include higher order effects and obtain normalized distributions.

Postgeneration we veto events without at least one lepton (photon) with transverse momentum $p_T(\ell) > 35$ GeV ($p_T(\gamma) > 15$ GeV and require a separation of $\Delta R(\ell,\gamma) > 0.7$. The azimuthal angles of the photon and the lepton are sorted by rapidity and $\Delta\phi_{\ell\gamma}$ is calculated similarly to the other channels.

We assume that the relative statistical and systematic errors that can be calculated from the measured cross section of Ref. [10],[1]

$$\sigma_{\text{fid}}(pp \to W\gamma \to \ell\nu) = 37.0 \pm 0.8(\text{stat}) \pm 4.0(\text{syst}) \pm 0.8(\text{lumi})\ \text{pb}, \quad (8)$$

will remain the same for the case of $\sqrt{s} = 13$ TeV and use this in the following statistical analysis.

B. Analysis of *CP*-sensitive observables

To study the allowed region of the $(C_{\tilde{W}}, C_{H\tilde{W}B})$ parameter space based on current experimental data at the LHC, we consider the differential distribution

$$\frac{d\sigma(C_{\tilde{W}}, C_{H\tilde{W}B})}{d\Delta\phi_X} = \frac{d\sigma_{\text{SM}}}{d\Delta\phi_X} + C_{\tilde{W}}\frac{d\sigma_{\tilde{W}}}{d\Delta\phi_X} + C_{H\tilde{W}B}\frac{d\sigma_{H\tilde{W}B}}{d\Delta\phi_X}, \quad (9)$$

where, depending on the process, $X = \ell' Z$, $\ell\ell$, $\ell\gamma$, and $\sigma_{H\tilde{W}B}$ and $\sigma_{\tilde{W}}$ are constructed from $Q_{H\tilde{W}B}$ and $Q_{\tilde{W}}$, respectively, and derive from MC integration of Eq. (5). We generate events for each process using the two coupling reference points $(C_{\tilde{W}}, C_{H\tilde{W}B}) = (1,0)$ and $(C_{\tilde{W}}, C_{H\tilde{W}B}) = (0,1)$ and can rescale distributions using the linear relation of Eq. (5) to subsequently scan over the space of the two *CP*-odd Wilson coefficients, performing a χ^2 fit, in order to obtain limits. The χ^2 statistics is defined as

$$\chi^2(C_{\tilde{W}}, C_{H\tilde{W}B}) = (b^i_{SM+d6}(C_{\tilde{W}}, C_{H\tilde{W}B}) - b^i_{\text{SM}}) \times V^{-1}_{ij}(b^j_{SM+d6}(C_{\tilde{W}}, C_{H\tilde{W}B}) - b^j_{\text{SM}}), \quad (10)$$

where $b^i_{SM+d6}(C_{\tilde{W}}, C_{H\tilde{W}B})$ is the number of events at a particular luminosity based on the ith bin of the differential distribution Eq. (9) for a set of Wilson coefficients and b^i_{SM} is the bin's expected number of events based solely on the SM. The covariance matrix V_{ij} includes the relative statistical and systematic uncertainties[2] from the experimental measurements, obtained from the aforementioned fiducial cross sections Eqs. (6)–(8) for each process and included in V_{ij} as terms of the form $(\varepsilon^2_{\text{rel stat}} + \varepsilon^2_{\text{rel syst}})b^i_{\text{SM}}b^j_{\text{SM}}$, assuming that both relative and systematic errors are fully correlated. $\varepsilon_{\text{rel stat}}$ and $\varepsilon_{\text{rel stat}}$ denote the relative statistical and systematic uncertainties of each process.

[1] ℓ for this cross section indicates each type of light lepton (e, μ) and not a sum over them.

[2] Luminosity uncertainties are treated as systematics.

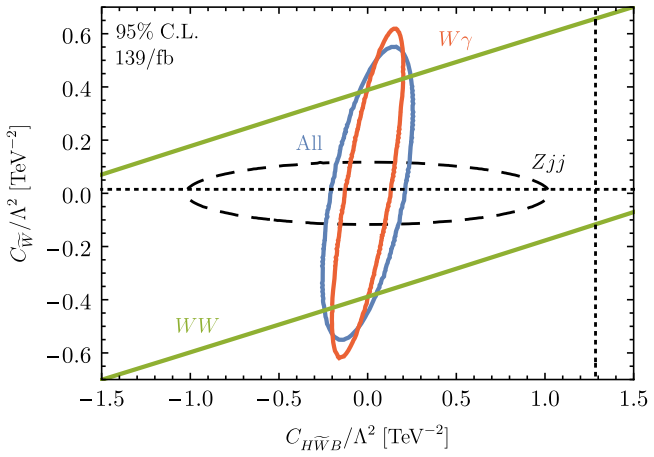

FIG. 1. Exclusion contours for $W\gamma$ and WW are shown separately and when combined for 139/fb. WZ does not provide significant sensitivity and lies outside the plotting region. We overlay the diboson constraints with the $Z+2j$ as extracted from the confidence intervals of ATLAS and the best fit lines (dotted) from experimental observations [4].

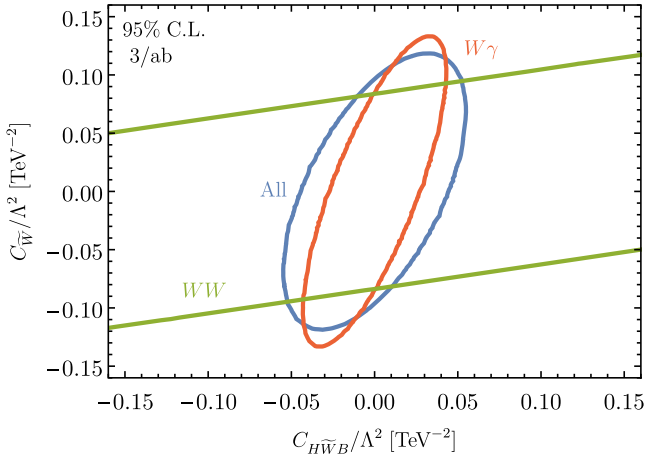

FIG. 2. Same as Fig. 1, but extrapolated to an integrated HL-LHC luminosity of 3/ab. The contours depend mostly on the statistical fluctuations and no significant change occurs when statistical errors are reduced.

We define the confidence intervals with

$$1-CL \geq \int_{\chi^2}^{\infty} \mathrm{d}x\, p_k(x), \qquad \chi^2 = \chi^2(C_{\tilde{W}}/\Lambda^2, C_{H\tilde{W}B}/\Lambda^2), \tag{11}$$

using the χ^2 distribution of k degrees of freedom $p_k(x)$, where k is obtained by subtracting the number of Wilson coefficients from the number of measurements.

We perform a scan based on an integrated luminosity of 139/fb to obtain the 95% confidence level contours shown in Fig. 1. The results are overlapped with the $Z+2j$ allowed region from ATLAS [4], as well as the best fit point from experimental data, while the WZ does not constrain the region enough to appear on the plot. To obtain the $Z+2j$ contours, we have tuned a covariance matrix on the basis of the information of Ref. [4] to obtain the exclusions reported in their work.

As can be seen the measurement of $Z+2j$ is considerably more sensitive to $Q_{\tilde{W}}$ than to $Q_{H\tilde{W}B}$, which results from a combination of accessing t-channel momentum transfers in the weak boson fusion-type selections and the Z boson having a larger overlap with the W^3 field than the photon. The latter is also the reason why $W\gamma$ production enhances the sensitivity in the $Q_{H\tilde{W}B}$ direction. We note that electroweak mono-photon production in association with two jets is more challenging due to jet-misidentification and thus does not provide significant sensitivity compared to prompt $W\gamma$ production.

C. HL-LHC extrapolation

We repeat the analysis with the same technique but using an integrated luminosity of 3/ab to obtain contours for HL-LHC. Systematic errors could be significantly reduced at HL-LHC; however, for this particular case, we find that the fact that BSM contributions are antisymmetric functions, in contrast to the symmetric SM differential distribution, leads to cancellations of the introduced errors in the χ^2.[3] Hence, the analysis is predominantly limited only by the statistical fluctuations. The extrapolated contours for 3/ab are shown in Fig. 2.

III. VECTORLIKE LEPTONS AS A MODEL FOR $C_{H\tilde{W}B}$-TARGETED (DI-)BOSON SIGNALS

Let us return to the examining the excess related to $Q_{H\tilde{W}B}$ from a UV model perspective. To this end, we extend the SM by three heavy vectorlike lepton (VLL) multiplets [32],

$$\Sigma_{L,R} = \begin{pmatrix} \eta \\ \xi \end{pmatrix}_{L,R} : (1,2,\mathcal{Y}), \qquad \eta'_{L,R} : \left(1,1,\mathcal{Y}+\frac{1}{2}\right),$$
$$\xi'_{L,R} : \left(1,1,\mathcal{Y}-\frac{1}{2}\right), \tag{12}$$

where the quantum numbers are depicted in $SU(3)_C \otimes SU(2)_L \otimes U(1)_Y$ convention.

The most-general gauge-invariant renormalizable Lagrangian involving these heavy VLLs can be written as

$$\begin{aligned}\mathcal{L}_{\mathrm{VLL}} = {} & \bar{\Sigma}(i\not{D}_{\Sigma} - m_{\Sigma})\Sigma + \bar{\eta'}(i\not{D}_{\eta'} - m_{\eta'})\eta' + \bar{\xi'}(i\not{D}_{\xi'} - m_{\xi'})\xi' \\ & - \{\bar{\Sigma}\tilde{H}(Y_{\eta_L}\mathbb{P}_L + Y_{\eta_R}\mathbb{P}_R)\eta' \\ & + \bar{\Sigma}H(Y_{\xi_L}\mathbb{P}_L + Y_{\xi_R}\mathbb{P}_R)\xi' + \mathrm{H.c.}\},\end{aligned} \tag{13}$$

[3]The same occurs if the absolute systematic errors are distributed according to a symmetric shape distribution across the bins, instead of using relative errors.

where m_Σ, $m_{\eta'}$, and $m_{\xi'}$ are the masses of Σ, η', and ξ', respectively. $\mathbb{P}_L(\mathbb{P}_R)$ are the left (right) chiral projection operator. Y_i's are the complex Yukawa couplings. We will consider $m_\Sigma = m_{\eta'} = m_{\xi'} = m$, i.e., all the VLLs are degenerate in this work.[4] We will see that this class of models provides the appropriate UV backdrop for the Wilson coefficient analysis that we have performed above and on which Ref. [4] relies.

A. Wilson coefficients

We integrate out all three heavy degenerate VLL multiplets; see Eq. (13) leading to the effective Lagrangian,

$$\mathcal{L}_{\rm EFT} = \mathcal{L}_{\rm SM} + \frac{1}{16\pi^2 m^2}\sum_i \mathcal{C}_i Q_i, \tag{14}$$

where Q_i, $\mathcal{C}_i$ denote the effective dimension six operators and the Wilson coefficients, respectively. The UV theory in Eq. (13) is suitably matched to the Standard Model effective field theory at the scale m which serves as the cutoff scale of the EFT. Here, the $16\pi^2$ factor signifies that all the effective operators are generated through one loop. And we separate off the loop factor $(16\pi^2)^{-1}$ from the definition of the Wilson coefficients $\mathcal{C}_i$, i.e., $C_i = \mathcal{C}_i/16\pi^2$ and $\Lambda = m$ in comparison with Eq. (3). We employ the modified minimal subtraction ($\overline{\rm MS}$) renormalization scheme and also set the RG scale at $\mu = m$. Integrating out heavy fermions from UV theories is discussed in Refs. [32,35]. Note that dimension eight *CP*-violating effects play a subdominant role when perturbative matching is possible in the first place; see [33,36]. We can therefore expect the dimension six deformations to play a dominant role.

We present the effective operators in the Warsaw basis [5] and their respective WCs are encapsulated in Table I. We also provide the matching using strongly interacting light Higgs (SILH)-like convention of [32] (see also [37,38]) in Table V of Appendix A for convenience. We compute the most generic results using the complete Lagrangian including *CP*-conserving and -violating interactions simultaneously. A subset of our generic results (in SILH-like basis) is in well agreement with operators computed in Ref. [32]. The results in WARSAW for this VLL scenario has been computed for the first time in this paper.[5] We find 19 effective operators with nonzero Wilson coefficients (16 *CP* even + 3 *CP* odd). In the renormalizable Lagrangian, the VLLs interact with the SM Higgs doublet and that explain the origin of ten bosonic along with nine fermionic effective operators accompanied by nonzero WCs. These appear due to application of the equation of motion of the SM Higgs doublet on the effective Lagrangian.

Here, we define the following functions to express the WCs in much more compact form [32] in Table I:

$$|\alpha_i|^2 = \frac{1}{4}(|Y_{i_L}|^2 + |Y_{i_R}|^2 + Y^*_{i_L}Y_{i_R} + Y_{i_L}Y^*_{i_R}), \tag{15}$$

$$|\beta_i|^2 = \frac{1}{4}(|Y_{i_L}|^2 + |Y_{i_R}|^2 - Y^*_{i_L}Y_{i_R} - Y_{i_L}Y^*_{i_R}), \tag{16}$$

where $i = \eta, \xi$. We further use the additional abbreviations for the same purpose [32],

$$\begin{aligned}
\mathcal{C}_F =& -\frac{2}{5}(|\alpha_\xi|^4 - 4|\alpha_\xi|^2|\alpha_\eta|^2 + |\alpha_\eta|^4) + \frac{4}{3}(|\beta_\eta|^4 + |\beta_\xi|^2|\beta_\eta|^2 + |\beta_\xi|^4)\\
&+ 2(|\alpha_\eta|^2|\beta_\eta|^2 + |\alpha_\xi|^2|\beta_\xi|^2) + \frac{2}{3}(|\beta_\xi|^2|\alpha_\eta|^2 + |\alpha_\xi|^2|\beta_\eta|^2)\\
&+ \frac{4}{3}((\alpha^*_\eta)^2\beta^2_\eta + \alpha^2_\eta(\beta^*_\eta)^2 + (\alpha^*_\xi)^2\beta^2_\xi + \alpha^2_\xi(\beta^*_\xi)^2) + \frac{4}{3}(\alpha_\xi\beta^*_\xi\alpha^*_\eta\beta_\eta + \alpha^*_\xi\beta_\xi\alpha_\eta\beta^*_\eta),\\
\mathcal{C}_{K4} =& \frac{1}{5}(|\alpha_\xi|^2 + |\alpha_\eta|^2) + \frac{1}{3}(|\beta_\xi|^2 + |\beta_\eta|^2),\\
\tilde{\mathcal{C}}_F =& \frac{1}{3}[(|Y_{\xi_L}|^2 + |Y_{\xi_R}|^2){\rm Im}[Y_{\xi_L}Y^*_{\xi_R}] - (|Y_{\eta_L}|^2 + |Y_{\eta_R}|^2){\rm Im}[Y_{\eta_L}Y^*_{\eta_R}]].
\end{aligned} \tag{17}$$

Here, we denote the electron (e)-, up (u)-, and down (d)-types Standard Model Yukawa couplings as $Y^e_{\rm SM}$, $Y^u_{\rm SM}$, and $Y^d_{\rm SM}$, respectively, while we refer to the SM Higgs quartic self-coupling as λ_H.

The operators that may affect the couplings of gauge bosons to fermion currents, i.e., the relevant LHC processes are [5,39,40]

$$Q_{eB}, \quad Q_{eW}, \quad Q_{uB}, \quad Q_{uW}, \quad Q_{dB}, \quad Q_{dW}, \tag{18}$$

$$Q^{(1)}_{Hl}, \quad Q^{(3)}_{Hl}, \quad Q^{(1)}_{Hq}, \quad Q^{(3)}_{Hq}, \quad Q_{Hud}, \quad Q_{He}, \quad Q_{Hu}, \quad Q_{Hd}. \tag{19}$$

[4]This model is also discussed in some detail in Refs. [32–34].

[5]In Ref. [32], the contributions from *CP*-violating (*CP*V) couplings into the *CP*-even operators are not considered.

TABLE I. The generated Warsaw basis operators and respective Wilson coefficients after integrating out VLLs using Eq. (13). The *CP*-odd gauge boson operators are displayed in first three rows. Multiplication with a common factor $(16\pi^2 m^2)^{-1}$ is understood implicitly; see Eq. (14).

Operators	Operator structures	Wilson coefficients ($\mathcal{C}_i$)
$Q_{H\tilde{B}}$	$(H^\dagger H)\tilde{B}_{\mu\nu}B^{\mu\nu}$	$-\frac{g_Y^2}{12}[(1+6\mathcal{Y}+12\mathcal{Y}^2)\mathrm{Im}[Y_{\eta_L}Y^*_{\eta_R}]+(1-6\mathcal{Y}+12\mathcal{Y}^2)\mathrm{Im}[Y_{\xi_L}Y^*_{\xi_R}]]$
$Q_{H\tilde{W}}$	$(H^\dagger H)\tilde{W}_{\mu\nu}{}^a W^{a,\mu\nu}$	$-\frac{g_W^2}{12}\mathrm{Im}[Y_{\eta_L}Y^*_{\eta_R}+Y_{\xi_L}Y^*_{\xi_R}]$
$Q_{H\tilde{W}B}$	$(H^\dagger\tau^a H)\tilde{W}_{\mu\nu}{}^a B^{\mu\nu}$	$\frac{g_W g_Y}{6}[(1+6\mathcal{Y})\mathrm{Im}[Y_{\eta_L}Y^*_{\eta_R}]+(1-6\mathcal{Y})\mathrm{Im}[Y_{\xi_L}Y^*_{\xi_R}]]$
Q_W	$\epsilon^{abc}W_\rho{}^{a,\mu}W_\mu{}^{b,\nu}W_\nu{}^{c,\rho}$	$g_W^3/180$
Q_H	$(H^\dagger H)^3$	$-\frac{2}{15}(\lvert\alpha_\eta\rvert^6+\lvert\alpha_\xi\rvert^6)+\frac{2}{3}(\lvert\beta_\eta\rvert^6+\lvert\beta_\xi\rvert^6)$ $+\frac{2}{3}(\lvert\alpha_\eta\rvert^4\lvert\beta_\eta\rvert^2+\lvert\alpha_\xi\rvert^4\lvert\beta_\xi\rvert^2)+2(\lvert\alpha_\eta\rvert^2\lvert\beta_\eta\rvert^4+\lvert\alpha_\xi\rvert^2\lvert\beta_\xi\rvert^4)$ $+\frac{2}{3}(\lvert\alpha_\eta\rvert^2((\alpha_\eta^*)^2\beta_\eta^2+\alpha_\eta^2(\beta_\eta^*)^2)+\lvert\alpha_\xi\rvert^2((\alpha_\xi^*)^2\beta_\xi^2+\alpha_\xi^2(\beta_\xi^*)^2))$ $+2(\lvert\beta_\eta\rvert^2((\alpha_\eta^*)^2\beta_\eta^2+\alpha_\eta^2(\beta_\eta^*)^2)+\lvert\beta_\xi\rvert^2((\alpha_\xi^*)^2\beta_\xi^2+\alpha_\xi^2(\beta_\xi^*)^2))$ $-2\lambda_H\mathcal{C}_F+\frac{4}{5}\lambda_H(\lvert\alpha_\xi\rvert^2+\lvert\alpha_\eta\rvert^2)+\frac{4}{3}\lambda_H(\lvert\beta_\xi\rvert^2+\lvert\beta_\eta\rvert^2)$
$Q_{H\Box}$	$(H^\dagger H)\Box(H^\dagger H)$	$-\frac{2}{5}(\lvert\alpha_\eta\rvert^2+\lvert\alpha_\xi\rvert^2)^2-\frac{1}{3}(\lvert\beta_\eta\rvert^2+\lvert\beta_\xi\rvert^2)^2$ $-\frac{1}{3}(\lvert\beta_\xi\rvert^2\lvert\alpha_\eta\rvert^2+\lvert\alpha_\xi\rvert^2\lvert\beta_\eta\rvert^2)-1(\lvert\alpha_\eta\rvert^2\lvert\beta_\eta\rvert^2+\lvert\alpha_\xi\rvert^2\lvert\beta_\xi\rvert^2)$ $-\frac{2}{3}(\alpha_\xi\beta_\xi^*\alpha_\eta^*\beta_\eta+\alpha_\xi^*\beta_\xi\alpha_\eta\beta_\eta^*)+\frac{1}{3}(\alpha_\eta^2(\beta_\eta^*)^2+(\alpha_\eta^*)^2\beta_\eta^2)$
Q_{HD}	$(H^\dagger\mathcal{D}_\mu H)^*(H^\dagger\mathcal{D}^\mu H)$	$-\frac{4}{5}(\lvert\alpha_\xi\rvert^2-\lvert\alpha_\eta\rvert^2)^2-\frac{2}{3}(\lvert\beta_\xi\rvert^2-\lvert\beta_\eta\rvert^2)^2$ $+\frac{2}{3}(\lvert\beta_\xi\rvert^2\lvert\alpha_\eta\rvert^2+\lvert\alpha_\xi\rvert^2\lvert\beta_\eta\rvert^2)-2(\lvert\alpha_\eta\rvert^2\lvert\beta_\eta\rvert^2+\lvert\alpha_\xi\rvert^2\lvert\beta_\xi\rvert^2)$ $+\frac{2}{3}(\alpha_\eta^2(\beta_\eta^*)^2+(\alpha_\eta^*)^2\beta_\eta^2)+\frac{4}{3}(\alpha_\xi\beta_\xi^*\alpha_\eta^*\beta_\eta+\alpha_\xi^*\beta_\xi\alpha_\eta\beta_\eta^*)$
Q_{HB}	$(H^\dagger H)B_{\mu\nu}B^{\mu\nu}$	$\frac{g_Y^2}{120}[(-7+40\mathcal{Y}-80\mathcal{Y}^2)\lvert\alpha_\xi\rvert^2+(-7-40\mathcal{Y}-80\mathcal{Y}^2)\lvert\alpha_\eta\rvert^2$ $+(5-40\mathcal{Y}+80\mathcal{Y}^2)\lvert\beta_\xi\rvert^2+(5+40\mathcal{Y}+80\mathcal{Y}^2)\lvert\beta_\eta\rvert^2]$
Q_{HW}	$(H^\dagger H)W_{\mu\nu}{}^a W^{a,\mu\nu}$	$-\frac{7g_W^2}{120}(\lvert\alpha_\xi\rvert^2+\lvert\alpha_\eta\rvert^2)+\frac{g_W^2}{24}(\lvert\beta_\xi\rvert^2+\lvert\beta_\eta\rvert^2)$
Q_{HWB}	$(H^\dagger\tau^a H)W_{\mu\nu}{}^a B^{\mu\nu}$	$\frac{g_W g_Y}{60}[(3-20\mathcal{Y})\lvert\alpha_\xi\rvert^2+(3+20\mathcal{Y})\lvert\alpha_\eta\rvert^2$ $+5(-1+4\mathcal{Y})\lvert\beta_\xi\rvert^2-5(1+4\mathcal{Y})\lvert\beta_\eta\rvert^2]$
Q_{eH}	$(H^\dagger H)(\bar{l}\ \mathrm{e}\ H)+\mathrm{H.c.}$	$-\frac{1}{2}\mathrm{Re}[(Y^e_{\mathrm{SM}})^\dagger]\mathcal{C}_F+\frac{1}{2}\mathrm{Im}[(Y^e_{\mathrm{SM}})^\dagger]\tilde{\mathcal{C}}_F+2\lambda_H(Y^e_{\mathrm{SM}})^\dagger(Y^e_{\mathrm{SM}})\mathcal{C}_{K4}$
Q_{uH}	$(H^\dagger H)(\bar{q}\ \mathrm{u}\ \tilde{H})+\mathrm{H.c.}$	$-\frac{1}{2}\mathrm{Re}[(Y^u_{\mathrm{SM}})^\dagger]\mathcal{C}_F-\frac{1}{2}\mathrm{Im}[(Y^u_{\mathrm{SM}})^\dagger]\tilde{\mathcal{C}}_F+2\lambda_H(Y^u_{\mathrm{SM}})^\dagger(Y^u_{\mathrm{SM}})\mathcal{C}_{K4}$
Q_{dH}	$(H^\dagger H)(\bar{q}\ \mathrm{d}\ H)+\mathrm{H.c.}$	$-\frac{1}{2}\mathrm{Re}[(Y^d_{\mathrm{SM}})^\dagger]\mathcal{C}_F+\frac{1}{2}\mathrm{Im}[(Y^d_{\mathrm{SM}})^\dagger]\tilde{\mathcal{C}}_F+2\lambda_H(Y^d_{\mathrm{SM}})^\dagger(Y^d_{\mathrm{SM}})\mathcal{C}_{K4}$
Q_{ledq}	$(\bar{l}^j\ \mathrm{e})(\bar{d}q_j)+\mathrm{H.c.}$	$\{(Y^e_{\mathrm{SM}})(Y^d_{\mathrm{SM}})^\dagger\mathcal{C}_{K4}+\mathrm{H.c.}\}$
$Q^{(1)}_{quqd}$	$(\bar{q}^j\ \mathrm{u})\epsilon_{\mathrm{jk}}(\bar{q}^k\ \mathrm{d})+\mathrm{H.c.}$	$\{(Y^u_{\mathrm{SM}})^\dagger(Y^d_{\mathrm{SM}})^\dagger\mathcal{C}_{K4}+\mathrm{H.c.}\}$
$Q^{(1)}_{lequ}$	$(\bar{l}^j\ \mathrm{e})\epsilon_{\mathrm{jk}}(\bar{q}^k\ \mathrm{u})+\mathrm{H.c.}$	$-\{(Y^e_{\mathrm{SM}})^\dagger(Y^u_{\mathrm{SM}})^\dagger\mathcal{C}_{K4}+\mathrm{H.c.}\}$
Q_{le}	$(\bar{l}\gamma_\mu\ \mathrm{l})(\bar{e}\gamma_\mu\ \mathrm{e})$	$-\frac{1}{2}(Y^e_{\mathrm{SM}})^\dagger(Y^e_{\mathrm{SM}})\mathcal{C}_{K4}$
$Q^{(1)}_{qu}$	$(\bar{q}\gamma^\mu\ \mathrm{q})(\bar{u}\gamma_\mu\ \mathrm{u})$	$-\frac{1}{2}(Y^u_{\mathrm{SM}})^\dagger(Y^u_{\mathrm{SM}})\mathcal{C}_{K4}$
$Q^{(1)}_{qd}$	$(\bar{q}\gamma_\mu\ \mathrm{q})(\bar{d}\gamma_\mu\ \mathrm{d})$	$-\frac{1}{2}(Y^d_{\mathrm{SM}})^\dagger(Y^d_{\mathrm{SM}})\mathcal{C}_{K4}$

We have a relevant *CP*-even operator Q_{HWB} that leads to an additional contribution to oblique corrections [41–48] and in particular the *S* parameter. In later section, we discuss the impact of all relevant *CP*-even operators in electroweak precision observables (EWPOs) in detail. At this point, it is worthy to mention that the operators

$$Q_{HB}, \qquad Q_{HW}, \tag{20}$$

$$Q_{H\tilde{W}}, \qquad Q_{H\tilde{B}} \tag{21}$$

do not modify trilinear gauge interactions as their contributions either vanish due to momentum conservation or can be absorbed into field and coupling redefinitions respecting gauge invariance. By investigating Table I, we also find that our adopted scenario, Eq. (13), predicts $\mathcal{C}_{\tilde{W}}=0$. Thus, together with our previous observations, we conclude that $Q_{H\tilde{W}B}\neq 0$ is the only relevant operator to interpret the results of ATLAS within the vectorlike lepton framework.

In passing, we would like to mention that some of the remaining nonzero operators can be probed in Higgs-boson

TABLE II. The *CP*-even effective operators (in Warsaw basis) after integrating out VLLs: "✓" and "✗" signify that the respective operator is constrained or not, respectively, by the EWPOs and Higgs data. The operators Q_{ledq}, $Q^{(1)}_{quqd}$, $Q^{(1)}_{lequ}$, Q_{le}, $Q^{(1)}_{qu}$, $Q^{(1)}_{qd}$ do not affect the observables under consideration.

Effective operators (Warsaw)	Constrained by EWPO	Constrained by Higgs data
Q_H	✓	✓
$Q_{H\Box}$	✓	✓
Q_{HD}	✓	✓
Q_{HB}	✗	✓
Q_{HW}	✗	✓
Q_{HWB}	✓	✓
Q_{eH}	✗	✓
Q_{uH}	✗	✓
Q_{dH}	✗	✓

TABLE III. Fitted values of the parameters, functions of Yukawa couplings of VLL model, using EWPOs and the Higgs data. The choice of the parameters is guided by the detailed structures of the Wilson coefficients; see Table I. We assume $m = 1$ TeV.

VLLs: Yukawa couplings	Fitted values of parameters (@ 68% C.L.)
$\mathrm{Re}[Y_{\eta_L} Y^*_{\eta_R}]$	$1.00^{+6.50}_{-4.10}$
$\mathrm{Im}[Y_{\eta_L} Y^*_{\eta_R}]$	$0.07^{+2.77}_{-1.20}$
$\mathrm{Re}[Y_{\xi_L} Y^*_{\xi_R}]$	$0.32^{+2.36}_{-4.51}$
$\mathrm{Im}[Y_{\xi_L} Y^*_{\xi_R}]$	$-9.9^{+15.0}_{-22.8}$
$\lvert Y_{\eta_L}\rvert^2$	$1.00^{+3.70}_{-1.00}$
$\lvert Y_{\eta_R}\rvert^2$	$0.65^{+5.48}_{-0.65}$
$\lvert Y_{\xi_L}\rvert^2$	$0.58^{+3.17}_{-0.58}$
$\lvert Y_{\xi_R}\rvert^2$	$1.30^{+3.10}_{-1.30}$

associated final states or (to a lesser extent) through their radiative correction contributions [49,50] (the latter corresponds to a two-loop suppression in the considered vectorlike lepton UV completion). These processes provide additional *CP* sensitivity, however, at smaller Higgs-boson related production cross sections (see, e.g., the discussion in Ref. [51]) that receive corrections from a range of nonzero Wilson coefficients $\mathcal{C}_{H\tilde{B}}$, $\mathcal{C}_{H\tilde{W}}$. We will not investigate Higgs-*CP* related effects in this work as neither they contribute to the electroweak precision observables nor impact the discussion of the previous section.[6]

B. Constraints from electroweak precision observables and Higgs data

The *CP*-even Standard Model effective field theory operators contribute to the EWPOs [39,54,55] and to the production and decay of the SM Higgs [56]. We note that all the dimension six operators, generated after integrating out the VLLs, do not leave any impact to these observables; see Table II. We briefly outline the nature of correlations among the relevant effective operators and the EWPOs in Appendix B. Though these observables do not constrain the *CP*-odd operators directly, we note that within our framework the *CP*-even and *CP*-odd operators are related to each other, see Tab. I, through the model parameters, e.g., the Yukawa couplings in Eq. (13). Here, we want to emphasize that instead of considering individual complex Yukawa couplings we prefer to work with a set of Yukawa functions, chosen based on the computed WCs; see Table III. This allows us to avoid unnecessary increase of free parameters in the theory which could have spoiled the quality of the fit without any gain for the earlier choice. Thus, by encapsulating the effects of these observables on *CP*-even WCs, we can deduce complementary constraints on the *CP*-odd WCs through the exotic Yukawa couplings in addition to the couplings' phases. We perform a detail χ^2-statistical analysis[7] using a *Mathematica* package OptEx [57] to estimate the allowed ranges of the model parameters in the light of the following experimental data: for EWPOs, see Table 2 of Ref. [58] and Higgs data for Run-1 ATLAS and CMS [59,60] and Run-2 ATLAS and CMS [59–70]. The statistically estimated parameters which are suitably chosen functions of VLL-Yukawa couplings are depicted in Table III.

IV. INDIRECT VECTORLIKE LEPTONS: FROM RUN-2 TO THE HL-LHC FRONTIER

In Fig. 3, we show a scan over the model parameters when contrasted with the parameter constraints of the ATLAS analysis result of Eq. (4). It can be seen that the large excess in the $C_{H\tilde{W}B}$ 95% constraint that is in tension with the SM favors either low mass scales or very large, potentially nonperturbative couplings. Direct searches for vectorlike leptons have been discussed in [71] and a HL-LHC direct coverage should be possible up to mass scales of 450 GeV which translates into model $\mathrm{Im}(Y_{i_L} Y^*_{i_R}) \sim 40$, thus probing $\mathrm{Re}(Y_i)$, $\mathrm{Im}(Y_i) \sim 6$. For such relatively low scales, where the EFT scale is identified with the statistical threshold of a particular analysis, the couplings are still in the strongly coupled, yet perturbative $|Y| \lesssim 4\pi$ regime. Such large couplings can lead to potential tension with

[6]The additional chiral symmetry violation that leads to nonvanishing Wilson coefficients could in principle be traced into a uniform modification of the Higgs two-point function [52] that can in principle be probed at hadron colliders. A related investigation was performed recently by CMS in four top final states [53]. Sensitivity, however, is currently too limited for this effect to play an important role in a global fit.

[7]We would like to mention that in our analysis the degree of freedom is 80 and p value is .36. The min-χ^2 is 83.86.

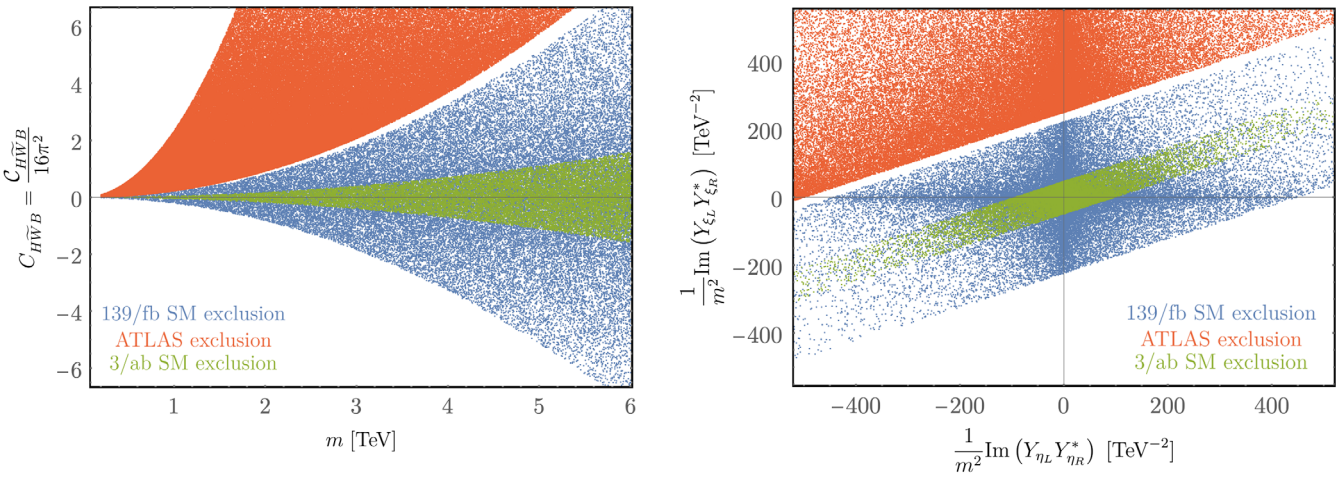

FIG. 3. On the left, $C_{H\tilde{W}B}$ Wilson coefficient calculated from the expression in Table I by sampling the Yukawa values and a fixed hypercharge of (SM-like) $\mathcal{Y} = -1/2$ is plotted against the vectorlike lepton mass m. On the right, the relevant combinations of Yukawa values contributing to $C_{H\tilde{W}B}$ are shown. The points for the different exclusions are determined by assessing whether $C_{H\tilde{W}B}/m^2$ lies within the 95% contours for 139/fb and 3/ab, as well as the allowed range the observed data of the ATLAS experiment [4].

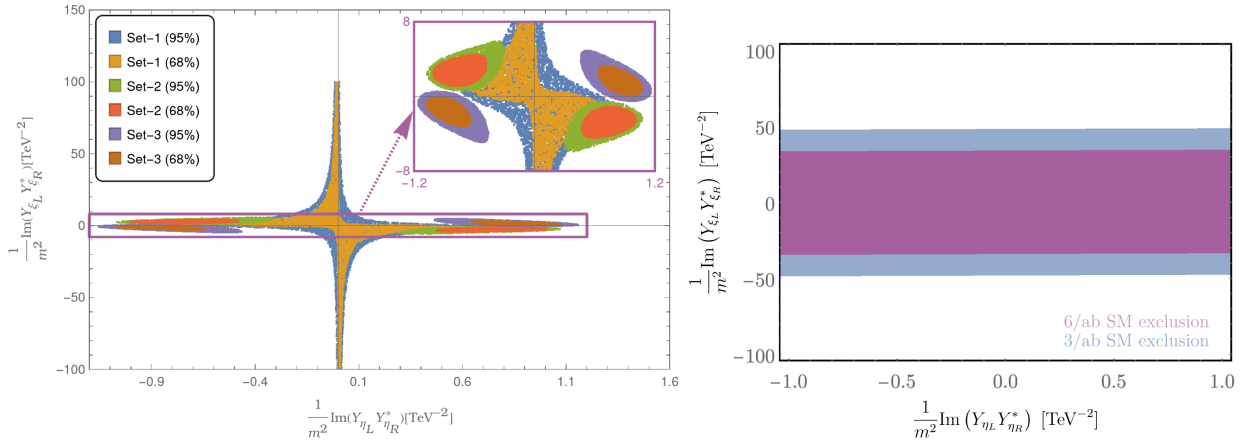

FIG. 4. Yukawa values allowed by the 68% and 95% C.L. fits using EWPOs and SM Higgs decays plotted along with the regions allowed from the diboson analysis with 3/ab. In addition, the diboson exclusions obtained for 6/ab (resulting from a ATLAS + CMS combination) with the same methodology are also included. The 68% and 95% C.L. fits are shown for three benchmark points (see Table IV).

other observables that are correlated through our particular model assumption. The constraints outlined in Sec. III B are in fact stronger, in particular for the combination of $\mathrm{Im}(Y_{\xi_L} Y^*_{\xi_R}) \lesssim 40$.

Returning to the complementary constraints that can be derived from the diboson, and in particular the $W\gamma$ analyses, we show the expected sensitivity range to the new physics scenario and its compatibility with the allowed parameter space consistent with the EWPO and Higgs signal strength in Fig. 4.[8] We choose three benchmark

TABLE IV. These are the three benchmark points chosen to analyze the 68% and 95% C.L. allowed parameter space in the $\mathrm{Im}[Y_{\eta_L} Y^*_{\eta_R}] - \mathrm{Im}[Y_{\xi_L} Y^*_{\xi_R}]$ plane, using the EWPO and the Higgs data. The shown fit parameters are set to the best-fit values (see Table I) and two other set of points. The corresponding 68% and 95% C.L. regions are shown in Fig. 4.

Fit parameters	Set 1 (best fit)	Set 2	Set 3
$\mathrm{Re}[Y_{\eta_L} Y^*_{\eta_R}]$	1.00	1.05	0.25
$\mathrm{Re}[Y_{\xi_L} Y^*_{\xi_R}]$	0.32	0.19	0.27
$\lvert Y_{\eta_L}\rvert^2$	1.00	0.61	0.73
$\lvert Y_{\eta_R}\rvert^2$	0.65	1.2	0.46
$\lvert Y_{\xi_L}\rvert^2$	0.58	0.38	0.52
$\lvert Y_{\xi_R}\rvert^2$	1.30	0.05	1.11

[8]It is important to note that while generating the EWPO + Higgs data consistent with parameter space, the *CP*-violating observables are not included.

points (see Tab. IV) and show the 65% and 95% C.L. regions in the $\mathrm{Im}[Y_{\eta_L} Y^*_{\eta_R}] - \mathrm{Im}[Y_{\xi_L} Y^*_{\xi_R}]$ plane. There it becomes clear that the searches outlined in the beginning of this work will provide important sensitivity to this particular model class in the future in the $\mathrm{Im}(Y_{\xi_L} Y^*_{\xi_R})$ direction, which (for our choice of $\mathcal{Y}$) is relatively unconstrained by Higgs and EWPO data.

V. DISCUSSION AND CONCLUSIONS

The insufficient amount *CP* violation in the SM to explain the observed matter-antimatter asymmetry is a clear indication of the presence of new physics beyond the SM. Consequently, analyses of *CP* properties of particle physics interactions are an important part of the current phenomenological program at various energies, reaching up to the current high-energy frontier explored at the LHC. The observation of $C_{H\tilde{W}B}$-related excess by the ATLAS Collaboration in the recent reference [4] could be the first indication of the presence of such interactions in the gauge boson-Higgs sectors. Taking inspiration from Ref. [4], the focus of this work is twofold which are as follows:

(i) We motivate a particular UV model class, namely, that of vectorlike leptons Eq. (13), to provide a minimal and consistent theoretical backdrop to the analysis of Ref. [4]. We perform a complete matching calculation at one-loop order and demonstrate that all relevant *CP*-odd EFT deformations of the SM amplitude of diboson (and $Z + 2j$) are dominantly captured by the $Q_{H\tilde{W}B}$ operator. In parallel, at the given order, we do not induce $Q_{\tilde{W}}$, which impacts the analyses of *CP*-odd observables in (di)boson final states as well, but which is consistent with the SM expectation of $C_{\tilde{W}} = 0$ given the results of Ref. [4]. The mass scales of the vectorlike lepton scenario that can be directly explored at the LHC [71] constrain the model's parameters to the strong coupling, yet perturbative regime. An analysis of electroweak precision and Run-2 Higgs results indicates that the region of the ATLAS excess could be explained by $\mathrm{Im}(Y_{\eta_L} Y^*_{\eta_R}) \simeq 0$ and a significant $\mathrm{Im}(Y_{\xi_L} Y^*_{\xi_R})$ with some tension given the UV-model's correlation of *CP*-even and *CP*-odd couplings for masses that fall into the HL-LHC kinematic coverage.

(ii) The excess observed by ATLAS deserves further scrutiny. We show that diboson analyses, and in particular $W\gamma$ production will serve as a strong cross check of the excess, in particular because its phenomenology is particularly sensitive to $Q_{H\tilde{W}B}$-induced deviations. The analysis suggested in Sec. II A will therefore allow the collaborations to directly explain the results of Ref. [4] as a statistical fluctuation or gather further, strong evidence for a non-SM source of *CP* violation.

Finally, the correlation of different Wilson coefficients as predicted by our matching calculation motivates additional Higgs-based phenomenology probe that can further constrain or solidify the excess through measurements that target, e.g., $Q_{H\tilde{B}}$, $Q_{H\tilde{W}}$ in a suitable way [51] (see also [72,73]).

ACKNOWLEDGMENTS

S. D. B. would like to thank Sunando Patra for the clarifications regarding the OptEx package and Anisha for helpful discussions on the statistical analysis. The work of S. D. B. and J. C. was supported by the Science and Engineering Research Board, Government of India, under the agreements SERB/PHY/2016348 (Early Career Research Award) and SERB/PHY/2019501 (MATRICS). The work of C. E. was supported by the UK Science and Technology Facilities Council (STFC) under Grants No. ST/P000746/1 and No. ST/T000945/1 and by the IPPP Associateship Scheme. The work of M. S. was supported by the STFC under Grant No. ST/P001246/1. The work of P. S. was supported by an STFC studentship under Grant No. ST/T506102/1.

APPENDIX A: WILSON COEFFICIENTS OF THE DIMENSION SIX EFFECTIVE OPERATORS IN THE SILH-LIKE BASIS

TABLE V. The complete set of most generic Wilson coefficients corresponding to the respective dimension six effective operators in the SILH-like basis (a part of the result is noted in Ref. [32]). The heavy VLL multiplets are integrated out from the UV complete theory. The WCs are calculated up to one-loop order considering the *CP*-conserving and -violating couplings simultaneously. Note down the additional contributions of *CP*V couplings to the *CP*-even operators. Note that we are referring to SILH-like operators as O_i, to highlight their difference from the Warsaw-basis operators.

Operators	Operator definition	Wilson coefficient ($\mathcal{C}_i$)
$\tilde{O}_f$	$\frac{i}{2}\lvert H\rvert^2((\mathcal{D}^2H)^\dagger H - H^\dagger\mathcal{D}^2H)$	$\frac{1}{3}[(\lvert Y_{\xi_L}\rvert^2+\lvert Y_{\xi_R}\rvert^2)\mathrm{Im}[Y_{\xi_L}Y^*_{\xi_R}] - (\lvert Y_{\eta_L}\rvert^2+\lvert Y_{\eta_R}\rvert^2)\mathrm{Im}[Y_{\eta_L}Y^*_{\eta_R}]]$
$\tilde{O}_{BB}$	$g_Y^2(H^\dagger H)\tilde{B}_{\mu\nu}B^{\mu\nu}$	$-\frac{1}{12}[(1+6\mathcal{Y}+12\mathcal{Y}^2)\mathrm{Im}[Y_{\eta_L}Y^*_{\eta_R}] + (1-6\mathcal{Y}+12\mathcal{Y}^2)\mathrm{Im}[Y_{\xi_L}Y^*_{\xi_R}]]$
$\tilde{O}_{WW}$	$g_W^2(H^\dagger H)\tilde{W}_{\mu\nu}{}^a W^{a,\mu\nu}$	$-\frac{1}{12}\mathrm{Im}[Y_{\eta_L}Y^*_{\eta_R}+Y_{\xi_L}Y^*_{\xi_R}]$
$\tilde{O}_{WB}$	$2g_Wg_Y(H^\dagger\tau^aH)\tilde{W}_{\mu\nu}{}^aB^{\mu\nu}$	$\frac{1}{12}[(1+6\mathcal{Y})\mathrm{Im}[Y_{\eta_L}Y^*_{\eta_R}] + (1-6\mathcal{Y})\mathrm{Im}[Y_{\xi_L}Y^*_{\xi_R}]]$
O_{3W}	$\frac{g_W^3}{3!}\epsilon^{\mathrm{abc}}W_\rho{}^{a,\mu}W_\mu{}^{b,\nu}W_\nu{}^{c,\rho}$	$\frac{1}{30}$
O_{2W}	$-\frac{g_W^2}{2}(\mathcal{D}^\mu W_{\mu\nu}{}^a)^2$	$\frac{2}{15}$
O_{2B}	$-\frac{g_Y^2}{2}(\partial^\mu B_{\mu\nu})^2$	$\frac{2+16\mathcal{Y}^2}{15}$
O_6	$(H^\dagger H)^3$	$-\frac{2}{15}(\lvert\alpha_\eta\rvert^6+\lvert\alpha_\xi\rvert^6)+\frac{2}{3}(\lvert\beta_\eta\rvert^6+\lvert\beta_\xi\rvert^6)-2\lambda_H\mathcal{C}_F$ $+\frac{2}{3}(\lvert\alpha_\eta\rvert^4\lvert\beta_\eta\rvert^2+\lvert\alpha_\xi\rvert^4\lvert\beta_\xi\rvert^2)+2(\lvert\alpha_\eta\rvert^2\lvert\beta_\eta\rvert^4+\lvert\alpha_\xi\rvert^2\lvert\beta_\xi\rvert^4)$ $+\frac{2}{3}(\lvert\alpha_\eta\rvert^2((\alpha_\eta^*)^2\beta_\eta^2+\alpha_\eta^2(\beta_\eta^*)^2)+\lvert\alpha_\xi\rvert^2((\alpha_\xi^*)^2\beta_\xi^2+\alpha_\xi^2(\beta_\xi^*)^2))$ $+2(\lvert\beta_\eta\rvert^2((\alpha_\eta^*)^2\beta_\eta^2+\alpha_\eta^2(\beta_\eta^*)^2)+\lvert\beta_\xi\rvert^2((\alpha_\xi^*)^2\beta_\xi^2+\alpha_\xi^2(\beta_\xi^*)^2))$
O_H	$\frac{1}{2}(\partial_\mu(H^\dagger H))^2$	$\frac{4}{5}(\lvert\alpha_\eta\rvert^2+\lvert\alpha_\xi\rvert^2)^2+\frac{2}{3}(\lvert\beta_\eta\rvert^2+\lvert\beta_\xi\rvert^2)^2$ $+\frac{2}{3}(\lvert\beta_\xi\rvert^2\lvert\alpha_\eta\rvert^2+\lvert\alpha_\xi\rvert^2\lvert\beta_\eta\rvert^2)+2(\lvert\alpha_\eta\rvert^2\lvert\beta_\eta\rvert^2+\lvert\alpha_\xi\rvert^2\lvert\beta_\xi\rvert^2)$ $+\frac{4}{3}(\alpha_\xi\beta_\xi^*\alpha_\eta^*\beta_\eta+\alpha_\xi^*\beta_\xi\alpha_\eta\beta_\eta^*)-\frac{2}{3}(\alpha_\eta^2(\beta_\eta^*)^2+(\alpha_\eta^*)^2\beta_\eta^2)$
O_T	$\lvert H^\dagger\mathcal{D}_\mu H\rvert^2$	$-\frac{4}{5}(\lvert\alpha_\xi\rvert^2-\lvert\alpha_\eta\rvert^2)^2-\frac{2}{3}(\lvert\beta_\xi\rvert^2-\lvert\beta_\eta\rvert^2)^2$ $+\frac{2}{3}(\lvert\beta_\xi\rvert^2\lvert\alpha_\eta\rvert^2+\lvert\alpha_\xi\rvert^2\lvert\beta_\eta\rvert^2)-2(\lvert\alpha_\eta\rvert^2\lvert\beta_\eta\rvert^2+\lvert\alpha_\xi\rvert^2\lvert\beta_\xi\rvert^2)$ $+\frac{2}{3}(\alpha_\eta^2(\beta_\eta^*)^2+(\alpha_\eta^*)^2\beta_\eta^2)+\frac{4}{3}(\alpha_\xi\beta_\xi^*\alpha_\eta^*\beta_\eta+\alpha_\xi^*\beta_\xi\alpha_\eta\beta_\eta^*)$
O_f	$\frac{1}{2}\lvert H\rvert^2(H^\dagger\mathcal{D}^2H+\mathrm{H.c.})$	$\mathcal{C}_F$
O_{K4}	$\lvert\mathcal{D}^2H\rvert^2$	$\frac{1}{5}(\lvert\alpha_\xi\rvert^2+\lvert\alpha_\eta\rvert^2)+\frac{1}{3}(\lvert\beta_\xi\rvert^2+\lvert\beta_\eta\rvert^2)$
O_{BB}	$g_Y^2(H^\dagger H)B_{\mu\nu}B^{\mu\nu}$	$\frac{1}{120}[(-7+40\mathcal{Y}-80\mathcal{Y}^2)\lvert\alpha_\xi\rvert^2+(-7-40\mathcal{Y}-80\mathcal{Y}^2)\lvert\alpha_\eta\rvert^2$ $+(5-40\mathcal{Y}+80\mathcal{Y}^2)\lvert\beta_\xi\rvert^2+(5+40\mathcal{Y}+80\mathcal{Y}^2)\lvert\beta_\eta\rvert^2]$
O_{WB}	$2g_Wg_Y(H^\dagger\tau^aH)(W_{\mu\nu}{}^aB^{\mu\nu})$	$\frac{1}{60}[(3-20\mathcal{Y})\lvert\alpha_\xi\rvert^2+(3+20\mathcal{Y})\lvert\alpha_\eta\rvert^2$ $+5(-1+4\mathcal{Y})\lvert\beta_\xi\rvert^2-5(1+4\mathcal{Y})\lvert\beta_\eta\rvert^2]$
O_{WW}	$g_W^2(H^\dagger H)W_{\mu\nu}{}^aW^{a,\mu\nu}$	$-\frac{7}{120}(\lvert\alpha_\xi\rvert^2+\lvert\alpha_\eta\rvert^2)+\frac{1}{24}(\lvert\beta_\xi\rvert^2+\lvert\beta_\eta\rvert^2)$
O_W	$ig_W(H^\dagger\tau^a\overleftrightarrow{\mathcal{D}^\mu}H)(\mathcal{D}^\nu W_{\mu\nu}{}^a)$	$\frac{4}{15}(\lvert\alpha_\xi\rvert^2+\lvert\alpha_\eta\rvert^2)+\frac{1}{3}(\lvert\beta_\xi\rvert^2+\lvert\beta_\eta\rvert^2)$
O_B	$\frac{i}{2}g_Y(H^\dagger\overleftrightarrow{\mathcal{D}^\mu}H)(\partial^\nu B_{\mu\nu})$	$\frac{4}{15}(\lvert\alpha_\xi\rvert^2+\lvert\alpha_\eta\rvert^2)+\frac{1}{3}(\lvert\beta_\xi\rvert^2+\lvert\beta_\eta\rvert^2)$

APPENDIX B: CORRECTIONS TO THE EWPOs FROM DIMENSION SIX WARSAW BASIS OPERATORS

The dimension six effective operators may affect the electroweak observables and modify the couplings related to the SM Higgs production and decay. These observables are very precisely measured. Thus, any alteration beyond their SM predicted values puts stringent constraints on the WCs associated with those operators.

The electroweak parameters under consideration are

$$\sin^2\theta_W = \frac{1}{2}\left(1-\sqrt{1-\frac{4\pi\alpha}{\sqrt{2}G_F m_Z^2}}\right), \qquad g_Y = \frac{\sqrt{4\pi\alpha}}{\cos\theta_W}, \qquad g_W = \frac{\sqrt{4\pi\alpha}}{\sin\theta_W},$$
$$g_Z = -\frac{g_W}{\cos\theta_W}, \qquad g_L^{\rm SM} = T_3 - Q\sin^2\theta_W, \qquad g_R^{\rm SM} = -Q\sin^2\theta_W,$$
$$\langle H\rangle = v_{ew} = \frac{1}{2^{1/4}\sqrt{G_F}}, \qquad m_W^2 = m_Z^2\cos^2\theta_W$$

and can be expressed as functions of the electroweak input parameters fine structure constant α, mass of Z boson m_Z, and Fermi constant G_F.[9]

Here, we capture the additional contributions to the EWPOs, the relevant parameters and couplings, following the prescription suggested in Refs. [39,54,55], in the presence of the computed dimension six operators in our VLL framework; see Table II. We estimate the contributions to the following parameters based on Refs. [39,54,55] (we denote the $SU(2)_L$, $U(1)_Y$ gauge couplings with g_W and g_Y, respectively):

(i) α and m_Z,

$$\delta\alpha = \frac{\alpha g_Y g_W C_{HWB}}{(g_Y^2+g_W^2)\Lambda^2}, \tag{B1}$$

$$\delta m_Z^2 = \frac{1}{2\sqrt{2}}\frac{m_Z^2}{G_F}\frac{C_{HD}}{\Lambda^2} + \frac{2^{1/4}\sqrt{\pi\alpha}m_Z}{G_F^{3/2}}\frac{C_{HWB}}{\Lambda^2}, \tag{B2}$$

respectively.

(ii) The Higgs boson mass m_H,

$$\delta m_H^2 = \frac{m_H^2}{\sqrt{2}G_F\Lambda^2}\left(-\frac{3C_H}{2\lambda_H} + 2C_{H\Box} - \frac{C_{HD}}{2}\right). \tag{B3}$$

(iii) The Weinberg angle (θ_W),

$$\delta(\sin^2\theta_W) = \frac{\sin 2\theta_W}{2\sqrt{2}\cos 2\theta_W G_F\Lambda^2} \times (\sin\theta_W C_{HD} + 2C_{HWB}). \tag{B4}$$

(iv) The gauge coupling (g_W),

$$\delta g_W = \frac{g_W}{2}\left(2\frac{\delta\alpha}{\alpha} - \frac{\delta(\sin^2\theta_W)}{\sin^2\theta_W}\right). \tag{B5}$$

(v) The couplings of fermions to charged gauge bosons,

$$\delta(g_W^l) = \delta(g_W^q) = \delta g_W. \tag{B6}$$

(vi) The mass and width of W boson,

$$\delta m_W = \frac{m_Z\cos\theta_W}{2}\left(\frac{2\delta g_W}{g_W}\right),$$
$$\delta\Gamma_W = \Gamma_W\left(\frac{4}{3}\delta g_W^l + \frac{8}{3}\delta g_W^q + \frac{\delta m_W^2}{2m_W^2}\right),$$

respectively.

(vii) The couplings of left (L) and right (R) chiral fermions to Z boson,

$$\frac{\delta g_Z}{g_Z} = -\frac{\delta m_Z^2}{2m_Z^2} + \frac{\sin\theta_W\cos\theta_W}{\sqrt{2}G_F\Lambda^2}C_{HWB},$$
$$\delta g_L^l = \delta(g_Z)g_L^l + g_Z\delta(\sin^2\theta_W), \qquad \delta g_L^\nu = \delta(g_Z)g_L^\nu, \qquad \delta g_R^l = \delta(g_Z)g_R^l, \qquad \delta g_R^\nu = 0,$$
$$\delta g_L^u = \delta(g_Z)g_L^u + \frac{2}{3}g_Z\delta(\sin^2\theta_W), \qquad \delta g_R^u = \delta(g_Z)g_R^u + \frac{2}{3}g_Z\delta(\sin^2\theta_W),$$
$$\delta g_L^d = \delta(g_Z)g_L^d + \frac{1}{3}g_Z\delta(\sin^2\theta_W), \qquad \delta g_R^d = \delta(g_Z)g_R^d.$$

[9] G_F gets correction from Q_{Hl} and Q_{ll} dimension six operators. In the case of the model of Eq. (13), these two operators are absent; thus, we directly impose $\delta G_F = 0$.

The total scattering cross section of Z boson,

$$\sigma^0_{had} = \frac{12\pi}{m_Z^2}\frac{\Gamma_e\Gamma_{had}}{\Gamma_Z^2},$$

including the effects of $\delta\Gamma_Z$, $\delta\Gamma_e$ and $\delta\Gamma_{had}$, $\delta\sigma_{had}$ can then be calculated straightforwardly. The partial decay width of the Z boson into fermions is given by

$$\Gamma_f = N_c\frac{m_Z}{12\pi}\sqrt{1-4\frac{m_f^2}{m_Z^2}}\left(\frac{1}{2}(g_L^2+g_R^2)+\frac{2m_f^2}{m_Z^2}\left(-\frac{g_L^2}{4}-\frac{g_R^2}{4}-\frac{3}{2}g_Lg_R\right)\right), \tag{B7}$$

where N_C is the color charge of the fermions. The change in the partial decay width is computed in a very similar way as done for $\delta\Gamma_W$. Furthermore, the ratios of the changes in partial decays, e.g., δR_l, δR_b, and δR_c, and the asymmetries (δA_f) and forward-backward (δA_{FB}^f) can be recast in terms of changes of the couplings.

[1] A. D. Sakharov, Pis'ma Zh. Eksp. Teor. Fiz. **5**, 32 (1967) [JETP Lett. **5**, 24 (1967)]; Usp. Fiz. Nauk **161**, 61 (1991) [Sov. Phys. Usp. **34**, 392 (1991)].
[2] G. Aad *et al.* (ATLAS Collaboration), Phys. Rev. Lett. **125**, 061802 (2020).
[3] A. M. Sirunyan *et al.* (CMS Collaboration), Phys. Rev. Lett. **125**, 061801 (2020).
[4] G. Aad *et al.* (ATLAS Collaboration), arXiv:2006.15458.
[5] B. Grzadkowski, M. Iskrzynski, M. Misiak, and J. Rosiek, J. High Energy Phys. 10 (2010) 085.
[6] K. Arnold *et al.*, Comput. Phys. Commun. **180**, 1661 (2009).
[7] J. Baglio *et al.*, arXiv:1404.3940.
[8] J. Bellm *et al.*, Eur. Phys. J. C **76**, 196 (2016).
[9] G. Aad *et al.* (ATLAS Collaboration), J. High Energy Phys. 09 (2011) 072.
[10] S. Chatrchyan *et al.* (CMS Collaboration), Phys. Rev. D **89**, 092005 (2014).
[11] C. J. Goebel, F. Halzen, and J. P. Leveille, Phys. Rev. D **23**, 2682 (1981).
[12] S. J. Brodsky and R. W. Brown, Phys. Rev. Lett. **49**, 966 (1982).
[13] R. W. Brown, K. L. Kowalski, and S. J. Brodsky, Phys. Rev. D **28**, 624 (1983); **29**, A2100 (1984).
[14] U. Baur, T. Han, and J. Ohnemus, Phys. Rev. D **48**, 5140 (1993).
[15] U. Baur, S. Errede, and G. L. Landsberg, Phys. Rev. D **50**, 1917 (1994).
[16] T. Han, AIP Conf. Proc. **350**, 224 (1995).
[17] H. Aihara *et al.*, arXiv:hep-ph/9503425.
[18] N. D. Christensen and C. Duhr, Comput. Phys. Commun. **180**, 1614 (2009).
[19] A. Alloul, N. D. Christensen, C. Degrande, C. Duhr, and B. Fuks, Comput. Phys. Commun. **185**, 2250 (2014).
[20] C. Degrande, C. Duhr, B. Fuks, D. Grellscheid, O. Mattelaer, and T. Reiter, Comput. Phys. Commun. **183**, 1201 (2012).
[21] J. Alwall, M. Herquet, F. Maltoni, O. Mattelaer, and T. Stelzer, J. High Energy Phys. 06 (2011) 128.
[22] P. de Aquino, W. Link, F. Maltoni, O. Mattelaer, and T. Stelzer, Comput. Phys. Commun. **183**, 2254 (2012).
[23] J. Alwall, R. Frederix, S. Frixione, V. Hirschi, F. Maltoni, O. Mattelaer, H. S. Shao, T. Stelzer, P. Torrielli, and M. Zaro, J. High Energy Phys. 07 (2014) 079.
[24] J. Alwall *et al.*, Comput. Phys. Commun. **176**, 300 (2007).
[25] V. Khachatryan *et al.* (CMS Collaboration), Phys. Lett. B **766**, 268 (2017).
[26] M. Aaboud *et al.* (ATLAS Collaboration), Eur. Phys. J. C **79**, 884 (2019).
[27] J. M. Campbell and R. K. Ellis, Phys. Rev. D **60**, 113006 (1999).
[28] J. M. Campbell, R. K. Ellis, and C. Williams, J. High Energy Phys. 07 (2011) 018.
[29] J. M. Campbell, R. K. Ellis, and W. T. Giele, Eur. Phys. J. C **75**, 246 (2015).
[30] R. Boughezal, J. M. Campbell, R. K. Ellis, C. Focke, W. Giele, X. Liu, F. Petriello, and C. Williams, Eur. Phys. J. C **77**, 7 (2017).
[31] J. Campbell and T. Neumann, J. High Energy Phys. 12 (2019) 034.
[32] A. Angelescu and P. Huang, J. High Energy Phys. 01 (2021) 049.
[33] T. Corbett, M. J. Dolan, C. Englert, and K. Nordström, Phys. Rev. D **97**, 115040 (2018).
[34] S. D. Bakshi, J. Chakrabortty, and S. K. Patra, Eur. Phys. J. C **79**, 21 (2019).
[35] S. A. R. Ellis, J. Quevillon, P. N. H. Vuong, T. You, and Z. Zhang, J. High Energy Phys. 11 (2020) 078.
[36] H. Bélusca-Maïto, A. Falkowski, D. Fontes, J. C. Romão, and J. a. P. Silva, J. High Energy Phys. 04 (2018) 002.
[37] G. F. Giudice, C. Grojean, A. Pomarol, and R. Rattazzi, J. High Energy Phys. 06 (2007) 045.
[38] R. Contino, M. Ghezzi, C. Grojean, M. Muhlleitner, and M. Spira, J. High Energy Phys. 07 (2013) 035.

[39] I. Brivio, Y. Jiang, and M. Trott, J. High Energy Phys. 12 (2017) 070.
[40] A. Dedes, W. Materkowska, M. Paraskevas, J. Rosiek, and K. Suxho, J. High Energy Phys. 06 (2017) 143.
[41] M. Golden and L. Randall, Nucl. Phys. **B361**, 3 (1991).
[42] B. Holdom and J. Terning, Phys. Lett. B **247**, 88 (1990).
[43] G. Altarelli and R. Barbieri, Phys. Lett. B **253**, 161 (1991).
[44] M. E. Peskin and T. Takeuchi, Phys. Rev. Lett. **65**, 964 (1990).
[45] B. Grinstein and M. B. Wise, Phys. Lett. B **265**, 326 (1991).
[46] G. Altarelli, R. Barbieri, and S. Jadach, Nucl. Phys. **B369**, 3 (1992); **B376**, 444(E) (1992).
[47] M. E. Peskin and T. Takeuchi, Phys. Rev. D **46**, 381 (1992).
[48] C. P. Burgess, S. Godfrey, H. Konig, D. London, and I. Maksymyk, Phys. Lett. B **326**, 276 (1994).
[49] C. Grojean, E. E. Jenkins, A. V. Manohar, and M. Trott, J. High Energy Phys. 04 (2013) 016.
[50] C. Englert and M. Spannowsky, Phys. Lett. B **740**, 8 (2015).
[51] F. U. Bernlochner, C. Englert, C. Hays, K. Lohwasser, H. Mildner, A. Pilkington, D. D. Price, and M. Spannowsky, Phys. Lett. B **790**, 372 (2019).
[52] C. Englert, G. F. Giudice, A. Greljo, and M. Mccullough, J. High Energy Phys. 09 (2019) 041.
[53] A. M. Sirunyan *et al.* (CMS Collaboration), Eur. Phys. J. C **80**, 75 (2020).
[54] S. Dawson and P. P. Giardino, Phys. Rev. D **101**, 013001 (2020).
[55] R. Alonso, E. E. Jenkins, A. V. Manohar, and M. Trott, J. High Energy Phys. 04 (2014) 159.
[56] C. W. Murphy, Phys. Rev. D **97**, 015007 (2018).
[57] S. Patra, sunandopatra/optex-1.0.0: Wo documentation (2019), https://doi.org/10.5281/zenodo.3404311.
[58] M. Baak, J. Cúth, J. Haller, A. Hoecker, R. Kogler, K. Mönig, M. Schott, and J. Stelzer, Eur. Phys. J. C **74**, 3046 (2014).
[59] G. Aad *et al.* (ATLAS and CMS Collaborations), J. High Energy Phys. 08 (2016) 045.
[60] G. Aad *et al.* (ATLAS Collaboration), Eur. Phys. J. C **76**, 6 (2016).
[61] G. Aad *et al.* (ATLAS Collaboration), Phys. Rev. D **101**, 012002 (2020).
[62] G. Aad *et al.* (ATLAS Collaboration), Eur. Phys. J. C **80**, 957 (2020).
[63] G. Aad *et al.* (ATLAS Collaboration), Phys. Lett. B **809**, 135754 (2020).
[64] G. Aad *et al.* (ATLAS Collaboration), Report No. ATLAS-CONF-2019-028.
[65] G. Aad *et al.* (ATLAS Collaboration), Report No. ATLAS-CONF-2020-007.
[66] M. Aaboud *et al.* (ATLAS Collaboration), Phys. Rev. D **97**, 072003 (2018).
[67] M. Aaboud *et al.* (ATLAS Collaboration), Phys. Lett. B **784**, 173 (2018).
[68] G. Aad *et al.* (ATLAS Collaboration), Phys. Lett. B **798**, 134949 (2019).
[69] A. M. Sirunyan *et al.* (CMS Collaboration), Eur. Phys. J. C **79**, 421 (2019).
[70] A. M. Sirunyan *et al.* (CMS Collaboration), J. High Energy Phys. 03 (2020) 131.
[71] N. Kumar and S. P. Martin, Phys. Rev. D **92**, 115018 (2015).
[72] D. Huang, A. P. Morais, and R. Santos, J. High Energy Phys. 01 (2021) 168.
[73] V. Cirigliano, A. Crivellin, W. Dekens, J. de Vries, M. Hoferichter, and E. Mereghetti, Phys. Rev. Lett. **123**, 051801 (2019).